Artificial Intelligence in the Life Sciences 3 (2023) 100058

Contents lists available at ScienceDirect

Artificial Intelligence in the Life Sciences

journal homepage: www.elsevier.com/locate/ailsci

Research Article

Discovery of novel $A_{2A}R$ antagonists through deep learning-based virtual screening

Miru Tang [a,b,c,#], Chang Wen [a,#], Jie Lin [a], Hongming Chen [a,*], Ting Ran [a,*]

[a] Division of Drug and Vaccine Research, Guangzhou Laboratory, Guangzhou 510530, China
[b] Bioland Laboratory (Guangzhou Regenerative Medicine and Health-Guangdong Laboratory), Guangzhou 510530, China
[c] State Key Laboratory of Respiratory Disease, Guangzhou Institutes of Biomedicine and Health, Chinese Academy of Sciences, Guangzhou 510530, China

ARTICLE INFO

Keywords:
Deep learning
Virtual screening
$A_{2A}R$ antagonist
Drug discovery
Molecular docking

ABSTRACT

The A_{2A} adenosine receptor ($A_{2A}R$) is emerging as a promising drug target for cancer immunotherapy. Novel $A_{2A}R$ antagonists are highly demanded due to few candidates entering clinic trials specific for cancer treatment. Structure-based virtual screening has made a great contribution to discover novel $A_{2A}R$ antagonists, but most depended on inefficient molecular docking on relatively small molecular databases. In this work, a deep learning strategy was applied to accelerate docking-based virtual screening, through which new structural types of $A_{2A}R$ antagonists for an extremely large molecular library were found successfully.

Introduction

In recent years, cancer immunotherapy has set off a new revolution in cancer treatment. The central idea is to promote or reactivate the immune response in immunosuppressive tumor microenvironment (TME) to kill tumor cells. Immune checkpoint inhibitors targeting cytotoxic T-lymphocyte-associated protein 4 (CTLA-4) and programmed cell death protein 1 (PD-1) have made great success in clinic treatment [1]. However, this immunotherapy does not always work because there are alternative immune mechanisms to control the immune response. Adenosine, an essential signaling molecule, is actually a key immunosuppressor, which can prevent an overzealous immune response under normal physiological conditions [2]. Within TME, high levels of adenosine inhibit the immune reaction toward tumor cells through activating the adenosine receptor-mediated immunosuppressive signaling in immune cells [3]. There are four types of adenosine receptors, namely A_1R, $A_{2A}R$, $A_{2B}R$, and A_3R. However, only $A_{2A}R$ and $A_{2B}R$ have immunosuppressive function. $A_{2A}R$ receives special attention as a target for cancer immunotherapy due to its high expression in immune cells and high affinity for adenosine [4]. Some early developed $A_{2A}R$ antagonists for neurological diseases indeed exhibit impressive anti-tumor effects when turning to cancers [5]. Recently, a series of novel $A_{2A}R$ antagonists have been developed specifically for cancer immunotherapy. They are effective in a variety of tumors by both monotherapy and combination, which represent a very promising strategy for cancer treatment. Some of them even showed dual antagonistic effects on $A_{2A}R$ and $A_{2B}R$ [6]. However, only several compounds have been processed to early phase clinical trials. Therefore, it is still necessary to develop novel $A_{2A}R$ antagonists to combat cancers.

Since the first antagonist co-crystal structure of $A_{2A}R$ was resolved, $A_{2A}R$ has become one of the best structurally characterized drug targets [7]. The structure data have led to the discovery of many highly active antagonists. Structure-based virtual screening made a special contribution to the discovery of novel $A_{2A}R$ antagonists. In the early days, Katritch et al. and Carlsson et al. applied this strategy to screen $A_{2A}R$ antagonists from millions of compounds [8,9]. Both of them obtained tens of new structural types of active compounds. In the following years, some other studies also proved the effectiveness of structure-based virtual screening in the discovery of $A_{2A}R$ antagonists [10–16], in particular by molecular docking methods. Recently, Wang et al. reported deep neural network (DNN) and convolutional neural network (CNN) based classification models which can accelerate this process [17]. After preparation using the deep learning models, the number of compounds used for final molecular docking was reduced by 90% and several potent $A_{2A}R$ antagonists were identified. In fact, a series of deep learning-based virtual screening methods [18,19] have been proposed in past few years and shown superior performance over traditional docking-based methods in terms of efficiency or scoring accuracy.

In this study, the Deep Docking algorithm reported by Gentile et al. [20] was particularly employed to search for $A_{2A}R$ antagonists, as it demonstrated up to 100-fold data reduction and 6000-fold enrichment of high scoring molecules in docking-based virtual screening. This

* Corresponding authors.
E-mail addresses: chen_hongming@gzlab.ac.cn (H. Chen), ran_ting@gzlab.ac.cn (T. Ran).
# The authors have equal contribution

https://doi.org/10.1016/j.ailsci.2023.100058
Received 26 November 2022; Received in revised form 13 January 2023; Accepted 18 January 2023
Available online 20 January 2023

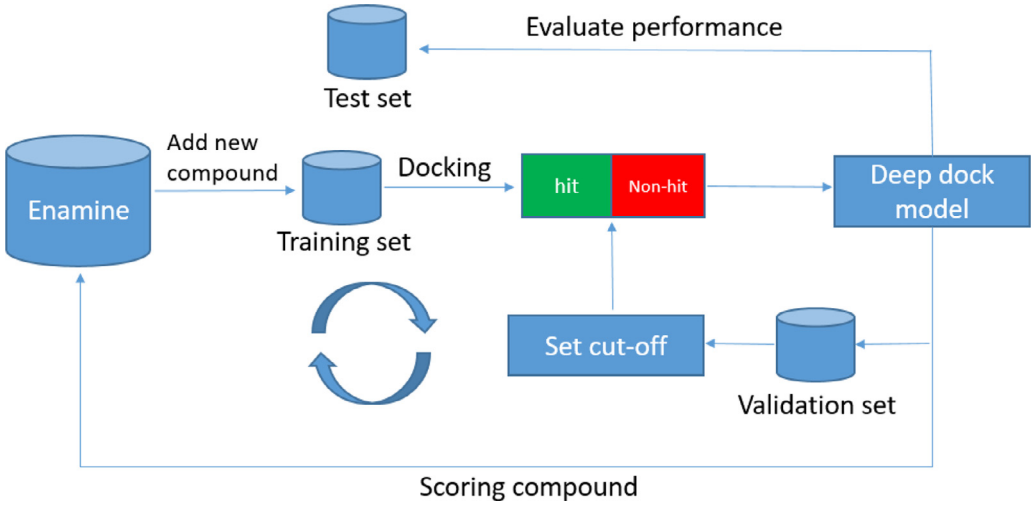

Fig. 1. Workflow of training Deep Docking model.

means it can achieve the screening of super large molecular library with minimal computational cost. Here, it was applied to screen the Enamine REAL library with 1.4 billion commercially available compounds. According to the Deep Docking protocol, a series of relatively small molecular subsets were first extracted from the library to iteratively train deep learning models to identify molecules with favorable scores as potential active compounds. Then, the model with the best performance on enrichment of true active compounds was used to predict the remaining molecules in the Enamine database. The molecules with high docking scores were then selected as virtual hits (VHs) and docked to the crystal structure of $A_{2A}R$ receptor and automatically filtered with pharmacophore models which characterized the binding modes of known $A_{2A}R$ antagonists. The filtered compound poses were further examined by visual inspection, which generated the final hit list for virtual screening. To validate the effectiveness of the computational method, tens of compounds were selected for in vitro assay and a series of novel $A_{2A}R$ antagonist was successfully identified. The screening results demonstrated the effectiveness of the Deep Docking method to accelerate virtual screening from a super large molecular library and the potential to facilitate traditional virtual screening.

Methods and materials

Data sources

The Enamine REAL library with 1.4 billion commercially available compounds were downloaded in SMILES format from the Enamine official website [21] for both model construction and virtual screening. The SMILES strings [22] were transformed to the Morgan fingerprints [23] for model training using the RDKit package under the environment of python 3.6. In addition, 1983 known $A_{2A}R$ antagonists were extracted from the ChEMBL database [24]for model evaluation.

Workflow for the construction of Deep Docking model

Gentile et al proposed a so called Deep Docking workflow to speed up the virtual screening on large databases. It is a docking-based deep learning model which is built on a multi-layer feed-forward neural network (FNN) to correlate the docking scores of molecules with molecular descriptors such as molecular fingerprints. The FNN model allows to identify molecules with favorable docking score purely through molecular descriptors and avoid the actual docking calculation. To improve model performance, its model training was designed as an iterative procedure through increasing the size of the training set step by step. In current study, model training followed similar workflow as Gentile's work (Figure 1). First of all, 1.5 million molecules were randomly sampled from the Enamine database and divided into three equal parts, namely training, validation and test sets. Molecules in each set were docked to the ligand-binding pocket of $A_{2A}R$ using Qvina docking method [25] to generate docking scores. These molecules were divided into virtual hit (VH) and non-VH by a docking score cut-off, which, at the beginning, was set to classify top S percentage (the boundary level) of scored molecules in the validation set as VH class and the remaining higher scored molecules (i.e. The docking score is a negative value) as non-VH class. To be noted, molecules failed in docking were discarded. The Morgan fingerprints of molecules in the training set were used to train the Deep Docking model. The model was then used to predict the probability of being VH for the rest of molecules in the Enamine database, so that the time consuming docking calculation for the large database can be spared. A probability threshold is set by ensuring 90% recovery of true VHs in the validation set (i.e. 90% VHs classified by docking score in validation set are correctly predicted by the model) and then the Deep Docking model classified compounds in database into VHs and non-VHs. Since second iteration, 0.5 million molecules (sample set) were randomly sampled from predicted VHs of last iteration and added into the training set to build a new model, while the validation and test set kept unchanged. The docking calculation was also done on the sample set for creating class labels and a lower score cut-off was applied to reassign class labels for molecules in the training set. The reduction of score cutoff was done by lowering the boundary level for molecules in the validation set, i.e. the top (S - m) percentage compounds were assigned to the VH class. The iterative process was terminated until the capability of the model to identify favorable scoring molecules could not be improved. In current study, the S was initially set to 1 and the m was set to 0.1.

In each iteration, 12 FNN models with various hyper-parameter were built for selection. The same hyper-parameters used in Gentile's work were employed in this study (Table S1). Specifically, maximum 500 epochs, learning rate of 0.0001 and a dropout frequency of 0.7 were used for all training runs. In addition, weight ratio for non-VH/VH class were set to either 2 or 3 to deal with the highly imbalanced nature of the data set (less than 1% VHs). The number of hidden layers in FNNs was set to either 2 or 3 and the number of neurons in each layer were set to 1000, 1500 and 2000 respectively.

Model evaluation

Deep Docking models were evaluated with normalized precision FPDE (full predicted database enrichment) which was calculated as the

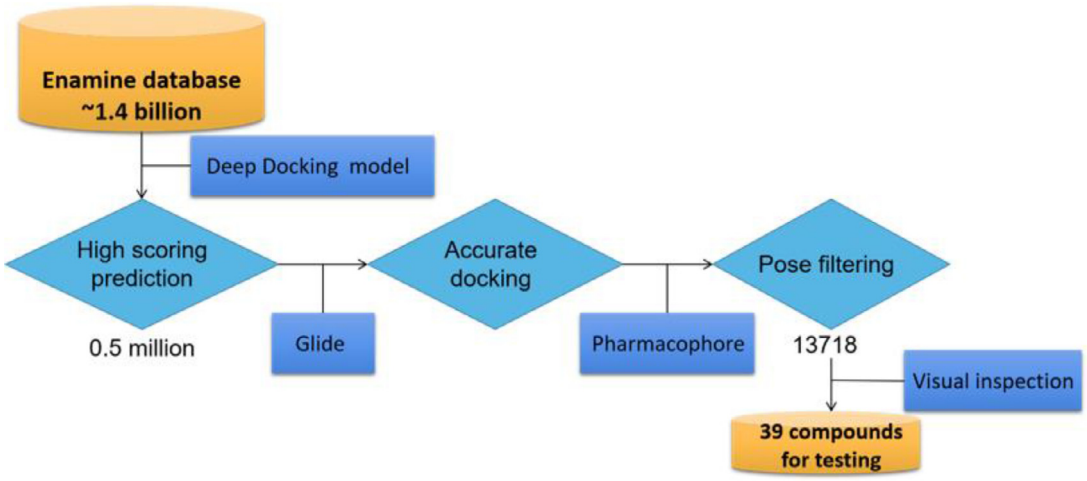

Fig. 2. Workflow of virtual screening using the Deep Docking model.

ratio between precision and random precision as shown in Eqs. 1-3, the random precision was calculated as the proportion of true VHs in test set. Another parameter for evaluation is recall, which were calculated as the percentage of true VHs in the predicted VHs and the proportion of true VHs correctly predicted by the model respectively. Here, the true VH refers to the molecule classified as VH class by their actual docking score in each iteration, while the predicted VH refers to the compound predicted to be VH by the Deep Docking model. On the other hand, the screening capability of Deep Docking model was evaluated using the area under the curve of Receiver Operating Characteristic (ROC-AUC) curve. Besides, enrichment factor (EF) was also computed to examine the enrichment of high scoring or known $A_{2A}R$ active molecules among the test set molecules sorted by the probability of being active in Deep Docking model. For calculation of EF, top 1% and 10% level were used for evaluation. Above mentioned metrics were calculated by following formulas:

$$\text{precision} = \frac{\text{true VHs}}{\text{total predicted VHs}} \tag{1}$$

$$\text{random precision} = \frac{\text{true VHs in test set}}{\text{total molecules in test set}} \tag{2}$$

$$\text{FPDE} = \frac{\text{precision}}{\text{random precision}} \tag{3}$$

$$\text{recall} = \frac{\text{true VHs}}{\text{total true VHs in the test set}} \tag{4}$$

$$\text{EF\_dockscore} = \frac{\text{true VHs in top N test set molecules}}{\text{true VHs in N randomly selected test set molecules}} \tag{5}$$

$$\text{EF\_active} = \frac{\text{active compounds hits in top N predicted VHs}}{\text{actual compounds in N randomly selected test set molecules}} \tag{6}$$

Workflow of deep learning-based virtual screening

The virtual screening of $A_{2A}R$ antagonists was shown in Figure 2. The final Deep Docking model for virtual screening was derived after four iterations of model training. It was used to select compounds from the whole Enamine database. Among the predicted VHs, the top 0.5 million molecules were selected for further Glide docking [26]. The Glide docking poses were further filtered by using pharmacophore models derived from X-ray complex structures of $A_{2A}R$ antagonists. The definition of pharmacophore features will be described in latter section. Furthermore, top 5000 docking poses passed the pharmacophore filtering were checked by visual inspection to select final compound list.

Qvina docking

Qvina docking software [25] was employed for Deep Docking model construction due to its particularly high efficiency in computation and high accuracy in reproduction of the crystal binding poses of different $A_{2A}R$ antagonists (Figure S1). At first, three-dimensional (3D) conformers of ligands were generated using the OMEGA [27] module in OpenEye software package. A co-crystal structure of $A_{2A}R$ (PDBID: 4EIY) with antagonist [28] was selected as docking receptor. The centroid of the crystal ligand was used to define the center of docking space. Only one docking pose was retained for each molecule and the binding energy was calculated as the docking score to evaluate molecules.

Glide docking

For the second stage of virtual screening, Glide docking method was employed [26]. The same protein structure was used as protein model. It was prepared using Protein Preparation Wizard module in Schrödinger software, in which a box with side length of 20 Å was centered on the crystal ligand and defined as the docking site by Receptor Grid Generation module. The protonation states of residues were generated at pH 7.0 using the Epik algorithm [29]. Ligands were prepared with the LigPrep module and Glide in standard precision mode (Glide-SP) was adopted for the docking. Maximal 10 docking poses were kept for each molecule. GlideScore was used as the docking score to evaluate binding affinity.

Building of pharmacophore model

To further filter docking results, pharmacophore models were constructed by combining key pharmacophore features of X-ray bound conformation of ligands. In total 21 co-crystal protein structures (Table S2) were retrieved from PDB database [30] and aligned in Maestro. The common features among the ligands were identified by comparing aligned ligand bound conformations. These features were recognized as key pharmacophore features for ligand binding and shown in Figure 3. They were then assembled into several hierarchical pharmacophore models (as shown in Table 2) for docking pose filtering.

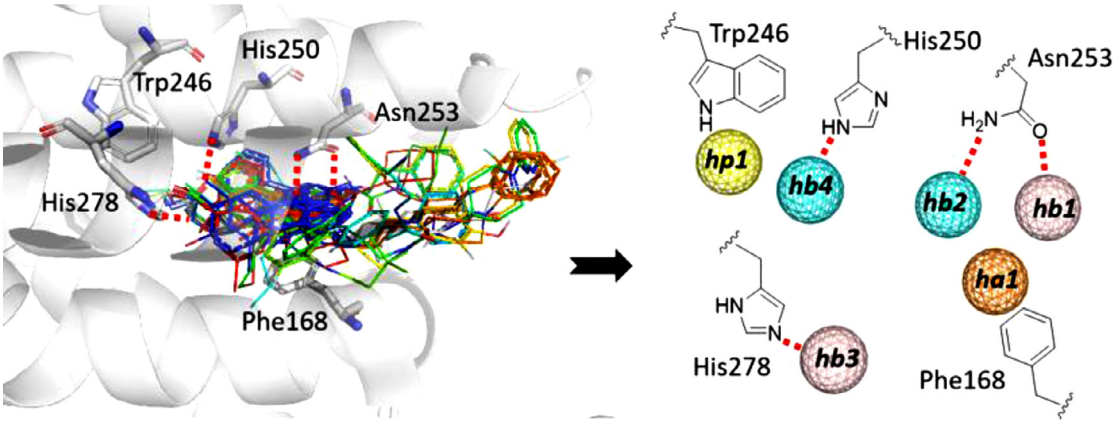

Fig. 3. Identification of key pharmacophore features for ligand binding. On the left, crystal ligands were aligned in the ligand-binding pocket of $A_{2A}R$ and shown as colored lines. Five critical residues (Phe168, Trp246, His250, Asn253 and His278) for ligand-binding were shown as white sticks. Red dashes represented key hydrogen bonds. On the right, colored spheres represented the key pharmacophore features of ligands which can form hydrogen bond interactions with the key residues. Orange and yellow spheres represented aromatic PI-PI and hydrophobic interaction features respectively, while pink and cyan spheres represented hydrogen bond donor and acceptor features respectively.

Table 1
The results of Deep Docking models.

Iteration	Best model no.	Recall	AUC	FPDE	Number of VHs in last round
1	7	0.9119	0.9067	3.5574	470403227
2	11	0.9116	0.9262	4.3823	98043324
3	11	0.9020	0.9290	4.5798	63126772
4	8	0.9026	0.9286	4.7902	57221642

Table 2
Enrichment of active compounds and true VHs (VHs) in the predicted VHs of test set.

Iteration	EF_active (0.01)	EF_active (0.1)	True VHs	True VHs (0.01)	EF_dockingscore (0.01)	True VHs (0.1)	EF_dockingscore (0.1)
1	19.145	5.764	10103	1230	12.177	6363	6.298
2	16.100	5.532	10103	1399	13.850	7141	7.068
3	17.287	5.351	10103	1484	14.692	7341	7.266
4	16.204	6.115	4618	776	16.808	3461	7.495

In vitro assay

$A_{2A}R$ is a G protein coupled receptor (GPCR) located in the cell membrane. When bound with adenosine by its extracellular domain, the receptor is activated and then stimulates the release of cyclic adenosine monophosphate (cAMP) in cells. Based on this mechanism, a cellular assay named Ultra Lance cAMP (PerkinElmer, catalog no. TRF0262) was employed to determine cAMP produced by cells upon $A_{2A}R$ activation through time resolved fluorescence resonance energy transfer technique. In the reaction kit, Europium-labeled cAMP tracer complexes compete with cellular cAMPs to bind with the cAMP-specific antibodies labeled with Alexa Fluor 647 dye. In the absence of cellular cAMP, maximum fluorescence signal was generated at 665 nM. The cellular cAMP upon $A_{2A}R$ activation decrease the fluorescence signal, while antagonists can reverse this signal proportionally. The inhibition of $A_{2A}R$ antagonists was quantitatively evaluated through this method.

Results and discussion

Construction of Deep Docking model

In each iteration, 12 FNN models were trained and the model with highest FPDE value was considered as the best model for sampling compounds in each iteration and outputting the probability of being VH. Four iterations of model training were done and model performance was shown in Table 1. In general, the ROC-AUC values during all iterations were above 0.9, which means that the model in each iteration can largely predict the docking score (i.e. predict VHs via Deep Docking model) for molecules in the database and false positive rate was maintained at a low level. It seems that after four iterations the ROC-AUC values converged, so the model of the fourth round was taken as our final model. On the other hand, the docking score cut-off for discriminating VHs and non-hits, supposed to decrease step by step, kept at the same level in the first three iterations. This is because that more than 1% of VHs in validation set had the docking score lower than the cut-off value of -9.8 kcal/mol and the lowest docking score of molecules in validation set was -9.9 kcal/mol (Table S3). Therefore, lowering the boundary level of VHs in validation set could no longer reduce the cut-off value with more iterations. The FPDE result was gradually improved through iterative training and the recovery rate of VHs in test set seems irregular, but the values were always larger than 90% for all iterations. This was comparable to the predefined recovery rate in validation set and suggested that all models can be extended to external data set. Additionally, it was found that the number of predicted VHs from the VH list of last round was constantly decreased, which means the new models led to less VHs. This indicated that the model became more stringent in picking up lower scored compounds after iterative training. At last, the enrichment of true VHs in the test set at top 1% and 10% levels was investigated (Table 2). Obviously, true VHs tended to concentrate among the top ranked predicted VHs regarding the enrichment factors at both 1% and 10% level and in the last iteration, the EFs for VHs were the largest. Interestingly, all models demonstrated large power for enriching the known active compounds among the test set compounds, although not a single active compound was included in the training set.

Table 3
The number of post-docked molecules satisfied the different combinations of pharmacophore features.

Model	Pharmacophore features	Number of matched molecules
M1	hb1+hb2+ha1	13718
M2	hb1+hb2+ha1+hb3	205
M3	hb1+hb2+ha1+hb4	193
M4	hb1+hb2+ha1+hp1	7446
M5	hb1+hb2+ha1+hb3+hb4	19
M6	hb1+hb2+ha1+hb3+hp1	116
M7	hb1+hb2+ha1+hb4+hp1	513
M8	hb1+hb2+ha1+hb3+hb4+hp1	10

In the end, the model built in the fourth iteration was selected as our final model for carrying out virtual screening of $A_{2A}R$ antagonists due to its balance performance in all aspects.

Virtual screening

In order to find novel $A_{2A}R$ antagonists, virtual screening on the Enamine REAL library was made using the above mentioned Deep Docking model. The predicted probability of being active was used to rank compounds in the database. The top 0.5 million molecules were further docked using Glide docking method and each molecule had maximal 10 docking poses, which were ranked by GlideScore. Then, eight pharmacophore models were built to filter out docking poses which doesn't fullfil the pharmacophore features (Table 3). Based on the alignment of crystal structures of $A_{2A}R$, two hydrogen bonds with Asn253 (i.e., hb1 and hb2) and one aromatic feature corresponding to the PI-PI stacking interaction with Phe168 (i.e., ha1) were found to be common for all $A_{2A}R$ antagonists. They were included in each pharmacophore model. Considering the different binding modes among the $A_{2A}R$ antagonists, the hydrogen bonds with His278 (hb3) and His250 (hb4) and the hydrophobic interaction with Trp246 (hp2) were optionally selected to combine with the common features, which resulted in seven pharmacophore models. After pharmacophore filtering, 13718 molecules which at least possessed three common pharmacophore features (hb1, hb2 and ha1) were remained. Among them, the number of molecules matching the hydrophobic feature hp1 was much larger than with other pharmacophore models. In fact, majority of known $A_{2A}R$ antagonists made hydrophobic interaction with Trp246. Only a few molecules matched all pharmacophore features. In the end, the top 3000 compounds among the 13718 compounds passing the pharmacophore filtering were selected and their docking poses were further checked by visual inspection, and 39 available molecules were finally ordered for activity validation. Their structures were shown in Table S4.

Activity validation

The activities of 39 compounds obtained by virtual screening were tested in vitro. Ultra Lance cAMP assay was employed to measure the inhibition of $A_{2A}R$-stimulated release of cAMP in cells. Repetition test at a single concentration of 10 μM identified two active compounds, namely Z1941887486 and Z4255667667 (Figure 4A/B). Both active compounds showed larger than 50% inhibition. Further test showed

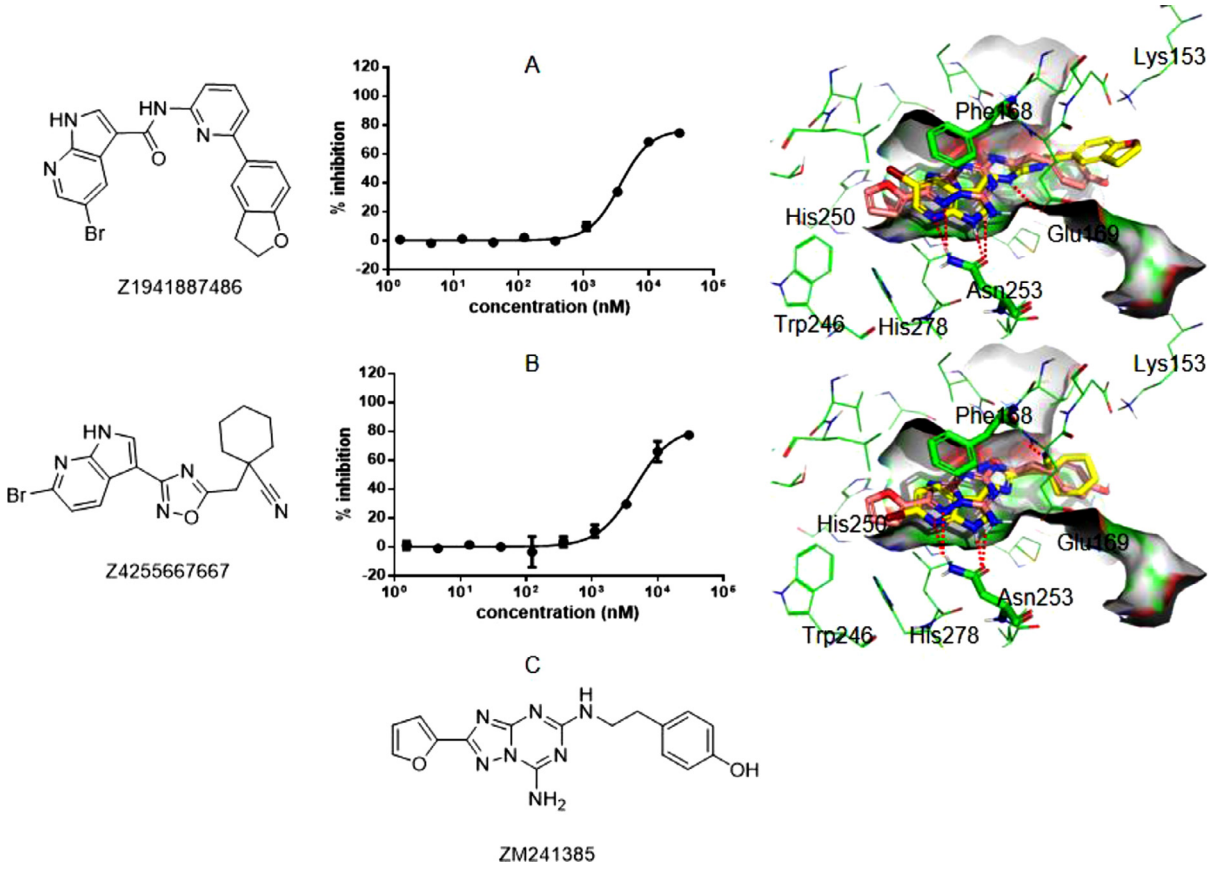

Fig. 4. Structure, inhibitory activity and binding mode of the compound Z1941887486 (A) and Z4255667667 (B). The inhibition was tested at different concentrations. The binding poses of Z1941887486 and Z4255667667 were respectively aligned with a known antagonist ZM241385, whose structure was shown in panel C. Z1941887486 and Z4255667667 were shown as yellow sticks, while ZM241385 was shown as pink sticks. Most residues were shown as green lines, while the critical residue Phe168 and Asn253 were shown as green sticks. The binding surface was also shown in the figure. Red dashes represent hydrogen bond interactions between compounds and residues.

that their half inhibitory concentration (IC_{50}) was 3.662 μM and 4.515, respectively. These two active compounds shared the same structural moiety which is novel comparing with known $A_{2A}R$ antagonists, their structures and predicted binding modes can be also seen in Figure 4A/B. They both have a pyrrolopyridine ring participate in the key hydrogen bonds with Asn153 and PI-PI stacking interaction with Phe168. Therefore, this molecular moiety can form hydrogen bond interactions with $A_{2A}R$. The fact that these two compounds have different bromide substituents on the pyrrolopyridine ring indicates that this structure moiety may be tolerant to various R-group decoration for further optimization. By analyzing their docking poses, it seems that the amide linker of Z1941887486 makes one hydrogen bond interaction with the side chain of Glu169, which appeared in some known antagonists. Z4255667667 misses this interaction, but could make one hydrogen bond with the backbone of Glu169 by its terminal nitrile group. At the entry of the pocket, Z1941887486 has a pyridine ring make aromatic interaction with Tyr271, while its terminal 2,3-dihydrobenzofuran substituent makes an additional hydrogen bond with Lys153. Z4255667667 just has a cyclohexane located at this place, which exhibits much difference in structure from Z1941887486. Compared to the known highly active compound ZM241385 [31] with similar binding mode (PDB code is 4EIY) (Figure 4C), which was also identified as positive compound by the model, these two compounds just have a bromine substitution located at the inner pocket formed by Trp246, His250 and His278, while ZM241385 has an aromatic substituent at this region. This may account for their relatively weaker activity and suggest a direction for further optimization of the hit structures.

Conclusion

Deep Docking is a novel deep learning workflow suitable for screening against super large molecular library. In this work, the method was applied to screen the Enamine REAL library with billions of compounds. Four iterations of model training were conducted, yielding high-quality Deep Docking models for virtual screening. The top ranked VHs based on the Deep Docking model went through a second round of Glide docking and the pharmacophore model-based filtering procedure. After manual inspection, 39 molecules were finally ordered for wet-lab test. In the follow-up in vitro assay, two compounds were confirmed to be $A_{2A}R$ hits and they possessed a novel scaffold. To our best knowledge, this is the first study to validate the effectiveness of the Deep Docking method on virtual screening. Looking back to the whole screening process, the deep learning model based on the docking of around 3 million compounds successfully helped us find two active compounds from the Enamine database instead of docking the entire molecular library which is much more computationally expensive.

Author contributions

H-M.C. directed the project and revised the manuscript. T.R. supervised the work, analyzed data and prepared the manuscript. M-R.T. and C.W. co-worked on the study and contributed equally to this work. J.L. wrote some python scripts in the program. All authors read and discussed the manuscript.

Declaration of Competing Interest

The authors declare no competing financial interest.

Data availability

Data will be made available on request.

Acknowledgments

This work was supported by Basic and Applied Basic Research Foundation of Guangzhou in 2021 and the National Natural Science Foundation of China under grants 21907081 in 2019.

Supplementary materials

Supplementary material associated with this article can be found, in the online version, at doi:10.1016/j.ailsci.2023.100058.

References

[1] Bagchi S, Yuan R, Engleman EG. Immune checkpoint inhibitors for the treatment of cancer: clinical impact and mechanisms of response and resistance. Annu Rev Pathol 2021;16:223–49.
[2] Antonioli L, Fornai M, Blandizzi C, Pacher P, Haskó G. Adenosine signaling and the immune system: when a lot could be too much. Immunol Lett 2019;205:9–15.
[3] Allard B, Allard D, Buisseret L, Stagg J. The adenosine pathway in immuno-oncology. Nat Rev Clin Oncol 2020;17(10):611–29.
[4] Muller-Haegele S, Muller L, Whiteside TL. Immunoregulatory activity of adenosine and its role in human cancer progression. Expert Rev Clin Immunol 2014;10(7):897–914.
[5] Jazayeri A, Andrews SP, Marshall FH. Structurally enabled discovery of adenosine A(2A) receptor antagonists. Chem Rev 2017;117(1):21–37.
[6] Yu F, Zhu C, Xie Q, Wang Y. Adenosine A(2A) receptor antagonists for cancer immunotherapy. J Med Chem 2020;63(21):12196–212.
[7] Jaakola VP, Ijzerman AP. The crystallographic structure of the human adenosine A2A receptor in a high-affinity antagonist-bound state: implications for GPCR drug screening and design. Curr Opin Struct Biol 2010;20(4):401–14.
[8] Katritch V, Jaakola VP, Lane JR, et al. Structure-based discovery of novel chemotypes for adenosine A(2A) receptor antagonists. J Med Chem 2010;53(4):1799–809.
[9] Carlsson J, Yoo L, Gao ZG, Irwin JJ, Shoichet BK, Jacobson KA. Structure-based discovery of A(2A) adenosine receptor ligands. J Med Chem 2010;53(9):3748–55.
[10] Congreve M, Andrews SP, Doré AS, et al. Discovery of 1,2,4-triazine derivatives as adenosine A(2A) antagonists using structure based drug design. J Med Chem 2012;55(5):1898–903.
[11] Langmead CJ, Andrews SP, Congreve M, et al. Identification of novel adenosine A(2A) receptor antagonists by virtual screening. J Med Chem 2012;55(5):1904–9.
[12] Bacilieri M, Ciancetta A, Paoletta S, et al. Revisiting a receptor-based pharmacophore hypothesis for human A(2A) adenosine receptor antagonists. J Chem Inf Model 2013;53(7):1620–37.
[13] Lenselink EB, Beuming T, Sherman W, van Vlijmen HW, IJ AP. Selecting an optimal number of binding site waters to improve virtual screening enrichments against the adenosine A2A receptor. J Chem Inf Model 2014;54(6):1737–46.
[14] Lenselink EB, Beuming T, van Veen C, et al. In search of novel ligands using a structure-based approach: a case study on the adenosine A(2A) receptor. J Comput Aided Mol Des 2016;30(10):863–74.
[15] Tian S, Wang X, Li L, et al. Discovery of novel and selective adenosine A(2A) receptor antagonists for treating parkinson's disease through comparative structure-based virtual screening. J Chem Inf Model 2017;57(6):1474–87.
[16] Lagarias P, Vrontaki E, Lambrinidis G, et al. Discovery of novel adenosine receptor antagonists through a combined structure- and ligand-based approach followed by molecular dynamics investigation of ligand binding mode. J Chem Inf Model 2018;58(4):794–815.
[17] Wang M, Hou S, Wei Y, Li D, Lin J. Discovery of novel dual adenosine A1/A2A receptor antagonists using deep learning, pharmacophore modeling and molecular docking. PLoS Comput Biol 2021;17(3):e1008821.
[18] Kimber TB, Chen Y, Volkamer A. Deep learning in virtual screening: Recent applications and developments. Int J Mol Sci 2021;22(9):4435.
[19] Rifaioglu AS, Atas H, Martin MJ, Cetin-Atalay R, Atalay V, Doğan T. Recent applications of deep learning and machine intelligence on in silico drug discovery: methods, tools and databases. Brief Bioinform 2019;20(5):1878–912.
[20] Gentile F, Agrawal V, Hsing M, et al. Deep Docking: A deep learning platform for augmentation of structure based drug discovery. ACS Cent Sci 2020;6(6):939–49.
[21] Enamine REAL Library; 2021. https://enamine.net/library-synthesis/real-compounds/. Accessed Sep 10 2022.
[22] Weininger D. SMILES, a chemical language and information system. 1. Introduction to methodology and encoding rules. J Chem Inf Comput Sci 1988;28(1):31–6.
[23] Morgan HL. The generation of a unique machine description for chemical structures-a technique developed at Chemical Abstracts service. J Chem Doc 1965;5(2):107–13.
[24] Mendez D, Gaulton A, Bento AP, et al. ChEMBL: Towards direct deposition of bioassay data. Nucleic Acids Res 2019;47(D1):D930–40.
[25] Alhossary A, Handoko SD, Mu Y, Kwoh C-K. Fast, accurate, and reliable molecular docking with QuickVina 2. Bioinformatics 2015;31(13):2214–16.
[26] Friesner RA, Banks JL, Murphy RB, et al. Glide: a new approach for rapid, accurate docking and scoring. 1. Method and assessment of docking accuracy. J Med Chem 2004;47(7):1739–49.
[27] Hawkins PCD, Skillman AG, Warren GL, Ellingson BA, Stahl MT. Conformer generation with OMEGA: Algorithm and validation using high quality structures

from the protein databank and Cambridge structural database. J Chem Inf Model 2010;50(4):572–84.
[28] Lebon G, Edwards PC, Leslie AG, Tate CG. Molecular determinants of CGS21680 binding to the human adenosine A2A receptor. Mol Pharmacol 2015;87(6):907–15.
[29] Shelley JC, Cholleti A, Frye LL, Greenwood JR, Timlin MR, Uchimaya M. Epik: a software program for pK(a) prediction and protonation state generation for drug-like molecules. J Comput Aided Mol Des 2007;21(12):681–91.
[30] Burley SK, Berman HM, Christie C, et al. RCSB Protein Data Bank: Sustaining a living digital data resource that enables breakthroughs in scientific research and biomedical education. Protein Sci 2018;27(1):316–30.
[31] Liu W, Chun E, Thompson AA, et al. Structural basis for allosteric regulation of GPCRs by sodium ions. Science 2012;337(6091):232–6.